Available online at www.eccomasproceedia.org
Eccomas Proceedia UNCECOMP (2025) 669-678

ECCOMAS
Proceedia

UNCECOMP 2025
6th ECCOMAS Thematic Conference on
Uncertainty Quantification in Computational Science and Engineering
M. Papadrakakis, V. Papadopoulos, G. Stefanou (eds.)
Rhodes Island, Greece, 15-18 June 2025

IDENTIFICATION OF THE LATERAL TRACK IRREGULARITIES FROM THE BEHAVIOR OF THE TRAIN'S AXLES ON A SURROGATE RAILWAY DYNAMICS MODEL

M.Chihaoui[1,2], D. Duhamel[1], C.Funfschilling[2] and G. Perrin[3]

[1]Laboratoire Navier, École nationale des ponts et chaussées
6 and 8 Avenue Blaise-Pascal, 77455 Champs-sur-Marne, France
e-mail: {malek.chihaoui,denis.duhamel}@enpc.fr

[2] SNCF, Direction Technologies, Innovation et Projets Groupe
1 to 9 Avenue François Mitterrand, 93210 Saint-Denis, France
e-mail: {malek.chihaoui,christine.funfschilling}@sncf.fr

[3]COSYS, Université Gustave Eiffel, 5 Boulevard Descartes, 77420 Champs-sur-Marne, France
e-mail: {guillaume.perrin}@univ-eiffel.fr

Abstract. *This work aims at the reverse identification of the lateral offset irregularity from the kinematics of the axle on a simplified train surrogate model. The fundamental goal of this study is to have a better understanding of the dynamics of the train which would ultimately allow to identify the track irregularities from axle-boxes acceleration measurements on commercial trains. First, a known surrogate model of the dynamics of the axle from the literature is adapted to include a train carbody and the railway track irregularities and then the inversion of the system is achieved so that a relationship between the kinematics that would be measured on the axle and the lateral track irregularity is established.*

Keywords: track irregularities, lateral offset, railway maintenance, inverse problem, linear estimation, train accelerations.

doi: 10.7712/120225.12385.25031

1 INTRODUCTION

Irregularities in railway tracks are critical factors that must be routinely monitored to maintain comfortable, safe, and punctual train operations. These geometrical irregularities and their classificatio is represented on figur 1. Additionally, understanding axle-rail contact forces and track irregularities is vital for analyzing the dynamic behavior and mechanical degradation of both trains and tracks. This data serves as a key input for various computational models, including those addressing rail and wheel damage, track settlement, and wheel wear.

Currently, specialized trains are used to measure and record track geometry, requiring dedicated personnel and equipment. Installing accelerometers on commercial trains and using the recorded accelerations to assess track geometry could enable more frequent and cost-effective monitoring, improving the organization and optimization of maintenance operations.

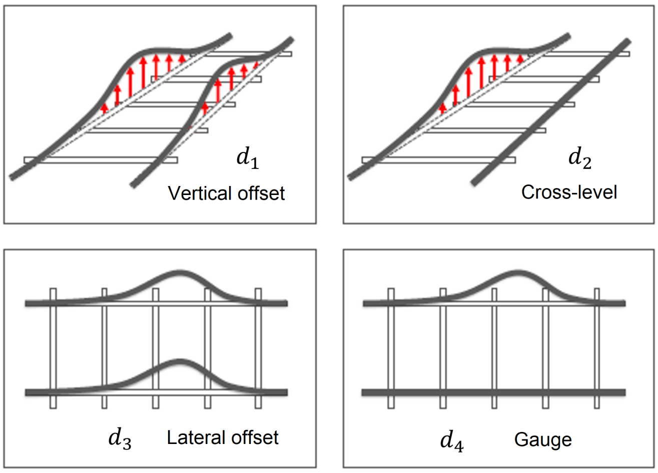

Figure 1: Classificatio of track geometric irregularities

Recent studies [1, 2, 3, 4], as well as a patent [5] have explored the reconstruction of vertical track irregularities using on-board accelerometers. This involves double integration of the measured accelerations, allowing the vertical track offset of each rail to be estimated from the vertical position of the corresponding wheel. However, this method cannot be directly applied to lateral track irregularities. This is because lateral movement of the train's axles is subject to a clearance (or play) in the wheel-rail contact, enabling the axles to shift laterally between the rails. Consequently, while lateral axle position is strongly influence by lateral irregularities, it cannot be directly inferred from them as it can for vertical irregularities. The axle's lateral dynamics between the tracks are complex, depending heavily on the train's mechanical properties and speed. Additionally, the train-track system exhibits significan non-linearity and is influence by various uncertainties, both internal (e.g., mass, suspension characteristics) and external (e.g., wind, rain), which further complicates the analysis.

In this work, the Klingel formulas [6], which describe the natural oscillations of axles on rails, are utilized and adapted to develop a surrogate model for railway dynamics. A linear surrogate model is constructed, incorporating the train carbody and track geometry, including certain irregularities. Then, an analytical inversion of the system is performed, allowing the deduction of the lateral offset irregularity from both the axle's kinematics and the known track layout parameters. The relationship is also identifie using linear regression, and both estimators are then compared.

2 SURROGATE MODEL CREATION

2.1 Lone axle's dynamics on straight railway tracks

To begin, we consider a perfectly straight track with no geometrical defects. We focus on the kinematics of a single axle of mass m and inertia j along $\overrightarrow{z}$ with a conical wheel profil of constant conicity c, which is define from the wheel conicity angle α as $c = tan\alpha$ as shown on both figur 2 and 3. The conical profil of the wheels means that the rolling radius is not constant and changes according to the lateral position taken by the axle, as detailed in figur 2. When centered, the rolling radius is r_0. Moreover, the axle is subjected to a constant longitudinal speed

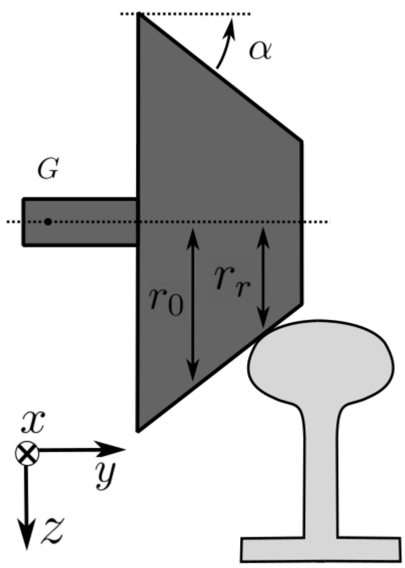

Figure 2: Rolling radius of the wheel

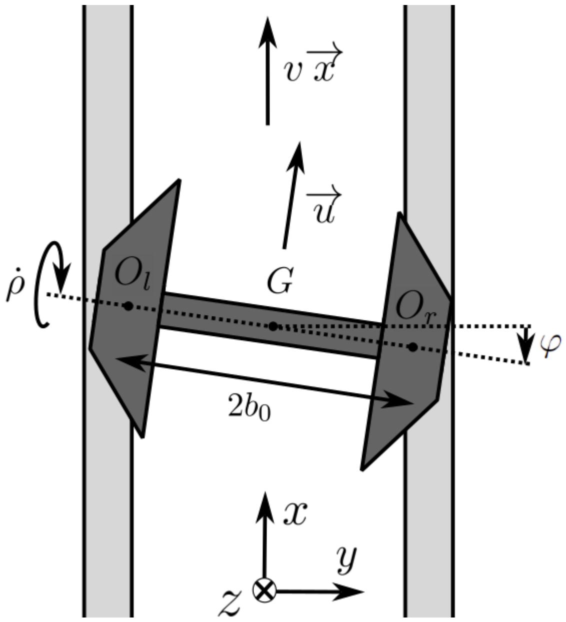

Figure 3: Diagram of the motion of the axle

$v\overrightarrow{x}$ and a constant wheel rotation speed $\dot{\rho} = \frac{v}{r_0}$. In order to take into account the interaction between the axle and the rail, it is necessary to calculate the friction forces and therefore identify the slip speed at each of the right and left wheels $\overrightarrow{v}_{slip,r/l}$. The full proof of how the creep force is obtained will not be detailed here, as it is well-documented in the literature [7, 8, 9]. However, a brief overview is provided. The relationship between the radius of each wheel and its lateral position enable to calculate the circumferential or rotation-induced speed of the contact point on the wheel at the contact interface $\overrightarrow{v}_{circ,r/l}$.

$$\overrightarrow{v}_{circ,r/l} = v(1 \pm \frac{c}{r_0}y)(\overrightarrow{x} + \varphi\overrightarrow{y}) \tag{1}$$

Whereas the translational speed at each contact interface $\overrightarrow{v}_{transl,r/l}$ is calculated using the kinematics of the axle, which is assumed not to roll but to slide perfectly on the rail.

$$\overrightarrow{v}_{transl,r/l} = (v \mp b_0\dot{\varphi})\overrightarrow{x} + \dot{y}\,\overrightarrow{y} \tag{2}$$

The slip speed is deduced from the difference between these two speeds at each wheel/rail interface points O_r and O_l which will be considered to be at a distance of b_0 from the axle's center of mass.

$$\overrightarrow{v}_{slip,r/l} = \overrightarrow{v}_{transl,r/l} - \overrightarrow{v}_{circ,r/l} = \mp(b_0\dot{\varphi} + \frac{vc}{r_0}y)\overrightarrow{x} + (\dot{y} - \varphi v)\overrightarrow{y} \tag{3}$$

The creep forces are computed on each wheel directly from the slip speeds using the linear Kalker creep law. κ_{11} and κ_{22} are respectively the longitudinal and lateral creep coefficients

$$\overrightarrow{F}_{creep,r/l} = -\frac{1}{v}\begin{bmatrix}\kappa_{11} & 0\\ 0 & \kappa_{22}\end{bmatrix}.\overrightarrow{v}_{slip,r/l} \tag{4}$$

These forces at each wheel create a lateral creep force as well as a momentumalong the vertical axis.

$$\begin{bmatrix}F_{creep}\\ M_{creep}\end{bmatrix} = -\begin{bmatrix}\frac{2\kappa_{22}}{v} & 0\\ 0 & \frac{2b_0^2\kappa_{11}}{v}\end{bmatrix}\begin{bmatrix}\dot{y}\\ \dot{\varphi}\end{bmatrix} - \begin{bmatrix}0 & -2\kappa_{22}\\ 2\kappa_{11}\frac{b_0 c}{r_0} & 0\end{bmatrix}\begin{bmatrix}y\\ \varphi\end{bmatrix} \tag{5}$$

Using Newton's second law of motion and this force, the dynamics equations governing a lone axle's movement can be deduced. This lateral dynamics surrogate model has been widely used in the literature, particularly for studying stability and calculating the critical speeds of trains. Typically, links to a virtual, motionless carbody centered between the rails are added, incorporating stiffness and damping elements. Indeed, with this model and at speeds below this critical speed, the axle tends to behave like a damped oscillator, swinging sideways before stabilizing in a centered lateral position.

2.2 Addition of the carbody, track parameters and irregularities

In our case, a free carbody with a lateral position of y_c and a yaw angle of φ_c of mass m_c and inertia j_c along $\overrightarrow{z}$ is added to the surrogate model. It is linked to the axle at each of the points $O_{r/l}$ with a longitudinal and a lateral stiffness K_x and K_y as well as a longitudinal and lateral damping C_x and C_y. These will create a lateral force and a torque along the vertical axis acting on both the axle and the carbody that can be written as follows :

$$\begin{bmatrix}F_{carbody/axle}\\ M_{carbody/axle}\end{bmatrix} = -\begin{bmatrix}F_{axle/carbody}\\ M_{axle/carbody}\end{bmatrix} = \begin{bmatrix}2C_y & 0\\ 0 & 2b_0^2C_x\end{bmatrix}\begin{bmatrix}\dot{y}-\dot{y}_c\\ \dot{\varphi}-\dot{\varphi}_c\end{bmatrix} + \begin{bmatrix}2K_y & 0\\ 0 & 2b_0^2K_x\end{bmatrix}\begin{bmatrix}y-y_c\\ \varphi-\varphi_c\end{bmatrix} \tag{6}$$

The next step involves incorporating the track layout parameters and irregularities into the model. These parameters will cause changes in the position of the rails along the curvilinear abscissa, affecting the creep forces. The relative lateral position of the axle in relation to the rail is denoted as y_r, which depends on the absolute lateral position of the axle y, the lateral offset irregularity d_3, and the effective roll of the rails θ_d, as shown in Figure 4.

$$y \simeq y_r + d_3 + r_0\theta_d \tag{7}$$

The track's effective cross-level angle θ_d, which incorporates both the track layout cross-level c_{track} and the irregularity d_2, is define by $\theta_d = \tan^{-1}(\frac{c_{track}+d_2}{2b_0})$. Since we are focusing on modeling only the lateral behavior of the train, the vertical offset and its irregularity d_1 will be ignored because their impact on the dynamics is purely vertical. Additionally, gauge irregularity d_4 will be disregarded for now, as it affects the system only through non-linearities [8]. The creep forces will then be computed using y_r instead of y in Equation 5.

$$\begin{bmatrix}F_{creep/axle}\\ M_{creep/axle}\end{bmatrix} = -\begin{bmatrix}\frac{2\kappa_{22}}{v} & 0\\ 0 & \frac{2b_0^2\kappa_{11}}{v}\end{bmatrix}\begin{bmatrix}\dot{y}_r\\ \dot{\varphi}\end{bmatrix} - \begin{bmatrix}0 & -2\kappa_{22}\\ 2\kappa_{11}\frac{b_0 c}{r_0} & 0\end{bmatrix}\begin{bmatrix}y_r\\ \varphi\end{bmatrix} \tag{8}$$

The last railways parameter to take into consideration is the curvature of the track γ. Since, the frame we are computing the inertias in is non-Galilean, the centrifugal force needs to be taken

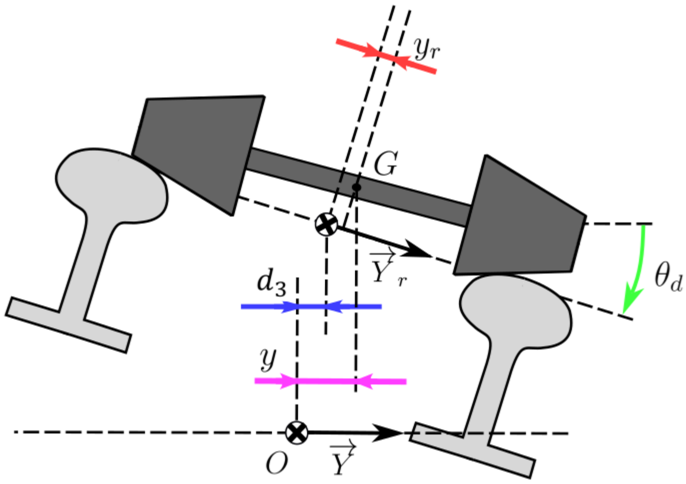

Figure 4: Diagram of the lateral motion of the axle

into consideration for both the axle and the carbody.

$$\begin{bmatrix} F_{centr/axle} \\ M_{centr/axle} \end{bmatrix} = \begin{bmatrix} -mv^2\gamma \\ -jv\dot{\gamma} \end{bmatrix}, \begin{bmatrix} F_{centr/carbody} \\ M_{centr/carbody} \end{bmatrix} = \begin{bmatrix} -m_c v^2\gamma \\ -j_c v\dot{\gamma} \end{bmatrix} \tag{9}$$

Adding up all the mentioned forces in equations 6, 8, and 9, a 4 degrees of freedom model is obtained :

$$\underline{\underline{\boldsymbol{M}}}\ddot{\underline{\boldsymbol{U}}} + \underline{\underline{\boldsymbol{C}}}\dot{\underline{\boldsymbol{U}}} + \underline{\underline{\boldsymbol{K}}}\underline{\boldsymbol{U}} = \underline{\underline{\boldsymbol{B}}}_2\dot{\underline{\boldsymbol{E}}} + \underline{\underline{\boldsymbol{B}}}_1\underline{\boldsymbol{E}}, \quad \underline{\boldsymbol{U}} = \begin{bmatrix} y \\ y_c \\ \varphi \\ \varphi_c \end{bmatrix}, \quad \underline{\boldsymbol{E}} = \begin{bmatrix} d_3 \\ \theta_d \\ \gamma \end{bmatrix} \tag{10}$$

The mass, damping, stiffness and forcing matrices are define as follows :

$$\underline{\underline{\boldsymbol{M}}} = \frac{1}{2}\begin{bmatrix} m & 0 & 0 & 0 \\ 0 & m_c & 0 & 0 \\ 0 & 0 & j & 0 \\ 0 & 0 & 0 & j_c \end{bmatrix}, \quad \underline{\underline{\boldsymbol{C}}} = \begin{bmatrix} C_y + \frac{\kappa_{22}}{v} & -C_y & 0 & 0 \\ -C_y & C_y & 0 & 0 \\ 0 & 0 & b_0^2(C_x + \frac{\kappa_{11}}{v}) & -b_0^2 C_x \\ 0 & 0 & -b_0^2 C_x & b_0^2 C_x \end{bmatrix} \tag{11}$$

$$\underline{\underline{\boldsymbol{K}}} = \begin{bmatrix} K_y & -K_y & -\kappa_{22} & 0 \\ -K_y & K_y & 0 & 0 \\ \kappa_{11}\frac{b_0 c}{r_0} & 0 & b_0^2 K_x & -b_0^2 K_x \\ 0 & 0 & -b_0^2 K_x & b_0^2 K_x \end{bmatrix}, \tag{12}$$

$$\underline{\underline{\boldsymbol{B}}}_1 = \begin{bmatrix} 0 & 0 & -\frac{1}{2}mv^2 \\ 0 & 0 & -\frac{1}{2}m_c v^2 \\ \kappa_{11}\frac{b_0 c}{r_0} & \kappa_{11} b_0 c & 0 \\ 0 & 0 & 0 \end{bmatrix}, \quad \underline{\underline{\boldsymbol{B}}}_2 = \begin{bmatrix} \frac{\kappa_{22}}{v} & \frac{\kappa_{22} r_0}{v} & 0 \\ 0 & 0 & 0 \\ 0 & 0 & -\frac{1}{2}jv \\ 0 & 0 & -\frac{1}{2}j_c v \end{bmatrix} \tag{13}$$

3 KINEMATICS AND INVERSION OF THE SYSTEM

3.1 Measurable kinematical quantities

The resulting system has 4 degrees of freedom and 3 forcing parameters. The whole purpose of this study is to identify the lateral offset irregularity d_3 which is one of the forcing parameters or inputs to the system from axlebox acceleration measurements. Furthermore, an analysis of the identificatio of the axle's kinematics shows that the lateral position y and the roll of the axle θ can be deduced respectively from the lateral accelerations and the difference of vertical accelerations. However, identifying the axle's yaw angle φ using the difference in longitudinal accelerations is far more challenging, as its amplitude is very small and easily obscured by noise and sensor movements. In addition, the curvature γ will be considered known along the entire track. The axle's roll θ although not directly appearing in equation 10 can be used since it can be expressed using other parameters if the dynamical deformation of the rail is neglected. It is composed by the roll of the rail θ_d that incudes both the cross-level layout and the irregularity as well as the roll of the axle relative to the rail θ_r.

$$\theta = \theta_d + \theta_r \tag{14}$$

The relative roll θ_r as demonstrated in figur 5 is linked to the relative lateral displacement y_r through the following relation.

$$\theta_r = -\frac{c}{b_0} y_r \tag{15}$$

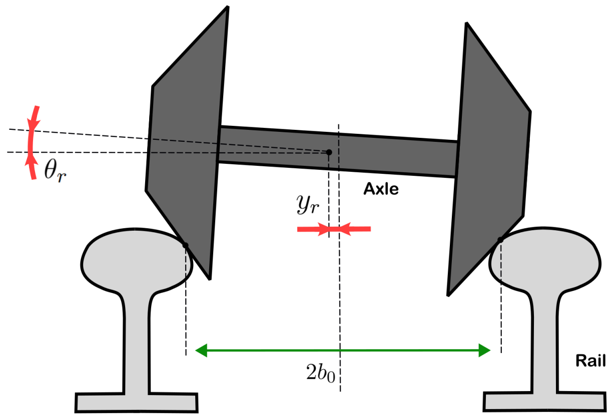

Figure 5: Diagram showing the isolated relative lateral displacement

3.2 System inversion

Let ω be the angular frequency and $\hat{\underline{U}}$ the Fourier transform of $\underline{U}$. With the use of the Fourier transform on equation 10 and with a matrix inversion, it can be written as follows :

$$\hat{\underline{U}} = (\underline{\underline{K}} - \omega^2 \underline{\underline{M}} + i\omega \underline{\underline{C}})^{-1} (\underline{\underline{B}}_1 + i\omega \underline{\underline{B}}_2) \hat{\underline{E}} \tag{16}$$

Extracting the firs line from this equation and noting $\underline{\underline{A}} = (\underline{\underline{K}} - \omega^2 \underline{\underline{M}} + i\omega \underline{\underline{C}})^{-1} (\underline{\underline{B}}_1 + i\omega \underline{\underline{B}}_2)$, The lateral position $\hat{y}$ can be written as such :

$$\hat{y} = \underline{\underline{A}}(1,1)\hat{d}_3 + \underline{\underline{A}}(1,2)\hat{\theta}_d + \underline{\underline{A}}(1,3)\hat{\gamma} \tag{17}$$

Using equations 7, 14and 15, θ_d is formulated as :

$$\theta_d = \frac{1}{1+\frac{r_0 c}{b_0}}\theta + \frac{\frac{c}{b_0}}{1+\frac{r_0 c}{b_0}} y - \frac{\frac{c}{b_0}}{1+\frac{r_0 c}{b_0}} d_3 \tag{18}$$

Then, 17 and 18 are combined and $\hat{d}_3$ is isolated. The transfer functions obtained are shown on figur 6.

$$\hat{d}_3 = \hat{H}_y.\hat{y} + \hat{H}_\theta.\hat{\theta} + \hat{H}_\gamma.\hat{\gamma} \tag{19}$$

The firs thing that stands out is the spikes that both $\hat{H}_y$ and $\hat{H}_\gamma$ reach around the wavelength $\lambda = 40m$. These spikes are linked to a known resonance phenomenon of trains which is the haunting oscillation. Then, one can notice that $\hat{H}_\theta$ has a constant norm and phase of π. This is due to the fact that d_3 and θ_d intervene in the same way in the equations and that $\underline{\underline{\boldsymbol{A}}}(1,1)$ and $\underline{\underline{\boldsymbol{A}}}(1,2)$ are the same up to a scaling factor.

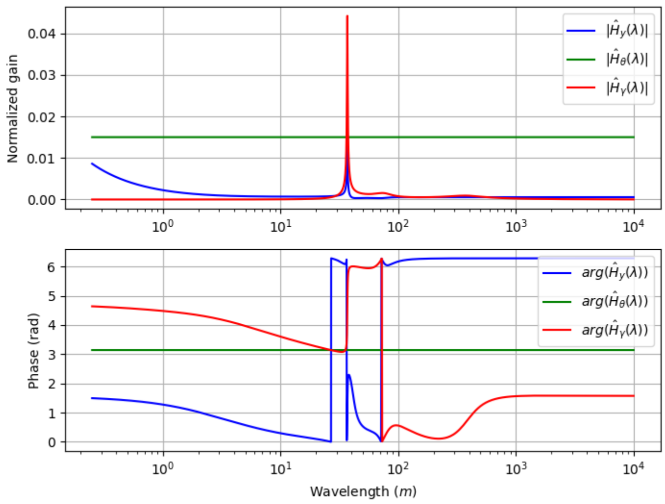

Figure 6: Theoretical transfer functions obtained by inverting the system

With the use of a reverse Fourier transform, the lateral offset irregularity d_3 at each point of the curvilinear abscissa s can be deduced by convolution from the two measured kinematics quantities y and θ as well as the known curvature γ and their corresponding kernels H_y, H_θ and H_γ which are the reverse Fourier transforms of the transfer functions $\hat{H}_y$, $\hat{H}_\theta$ and $\hat{H}_\gamma$. These convolution kernels are displayed on figur 7.

$$d_3 = H_y * y + H_\theta * \theta + H_\gamma * \gamma \tag{20}$$

The obtained kernels are very different from each others. As expected H_θ is a Dirac delta function. H_y and H_γ are however very different. H_y is discontinuous at the $s = 0$ and very limited in space as it gets close to null for $|s| > 50m$. This is the complete opposite for H_γ whose value diminishes very slowly as s decreases. This means that for these theoretical kernels to be used, they need to be very wide.

4 LATERAL TRACK IRREGULARITY IDENTIFICATION ON A NUMERICAL EXPERIMENT

A numerical experience is carried out where the reaction of the surrogate model to a real measured forcing is computed. Measured track irregularities d_2 and d_3 and track designs c_{track} and γ on the french railway network as well as realistic high speed train suspensions parameters, conicity and creep coefficient are employed. Then, the kernels derived from the system

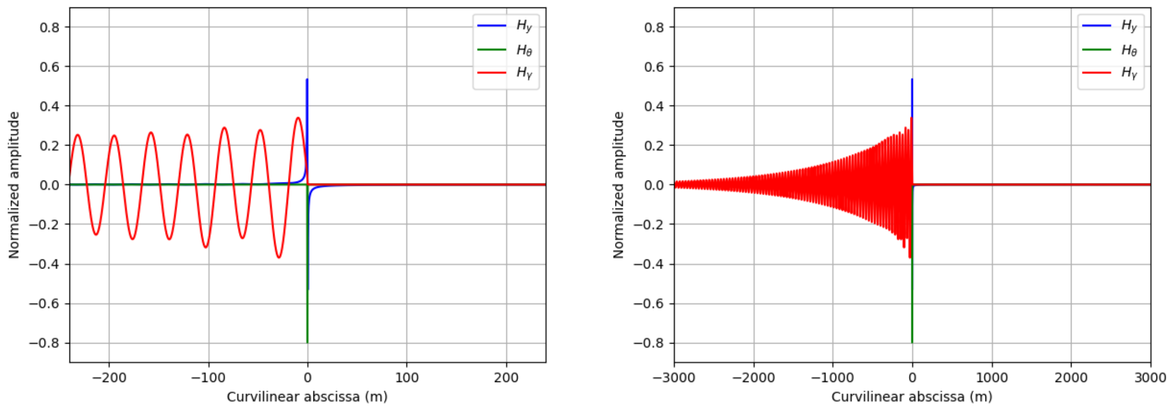

Figure 7: Theoretical kernels obtained by inverting the system

inversion are used to try to estimate the lateral offset irregularity d_3. These kernels were found to give a precise estimation only if their half width l is large enough as the lateral offset identifi cation requires the knowledge of the track curvature γ for a long distance as it appears on 7. For half widths of $300m$ and $1000m$, respective RMS errors of $3.4mm$ and $1.9mm$ are found. An identificatio error of $\epsilon_{d_3} = 0.25mm$ is only obtained for kernels with a half width of at least $3000m$. These errors are summarized on table 1.
On the other hand, the kernels can also be identifie using a linear regression algorithm. For this purpose, ridge regression with a regularization parameter α has been chosen as it gives the most accurate results. let $X = (y, \theta, \gamma)$. The ridge kernels are obtained as follows :

$$H_{ridge} = argmin_H \left\{ \sum_s |d_3(s) - H.X[s-l, s+l]|^2 + \alpha |H|^2 \right\} \tag{21}$$

The kernels given by this method give good estimations of the lateral offset irregularity d_3 with much smaller half widths. with $l = 300m$ and $1000m$ we obtain respective RMS identificatio errors of $0.1mm$ and $0.03mm$ which should be compared to the RMS value of the lateral offset irregularity in the database used $RMS(d_3) = 2mm$. The ones with a half-width of $l = 1000m$ are shown on 8 and the identificatio of the lateral offset irregularity is on figur 9. The obtained kernels closely resemble the theoretical ones, but they appear as if noise has been added. In fact, since they are constructed based on statistical correlation, they depend not only on the dynamics equation but also on the characteristics of the given input signals. Unlike the theoretical kernels, they are also adapted to the chosen half-width and with $l = 1000m$ the identificatio of d_3 is practically perfect.

Kernels used	Theoretical	Theoretical	Theoretical	Ridge regression	Ridge regression
Half width $l(m)$	300	1000	3000	300	1000
RMSE $\epsilon_{d_3}(mm)$	3.4	1.9	0.24	0.10	0.03

Table 1: Summary of the RMS identificatio errors of d_3

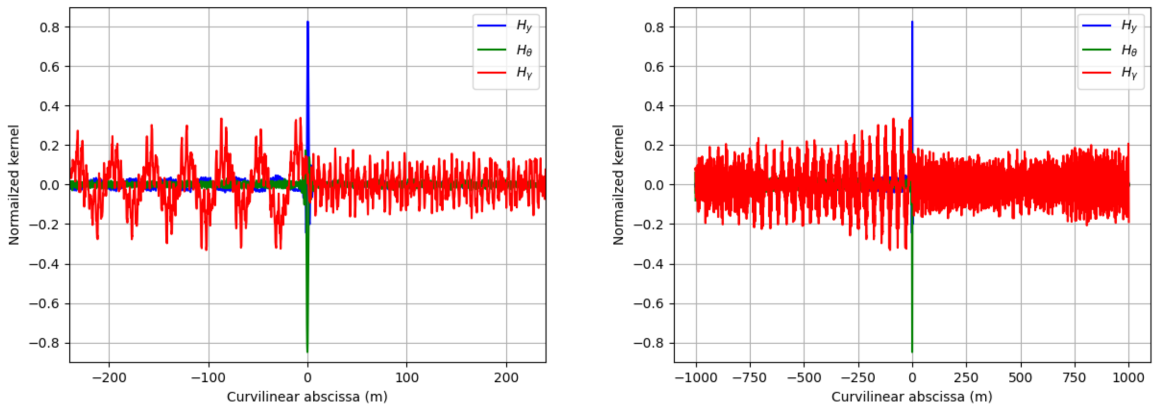

Figure 8: Empirical kernels obtained by Ridge regression

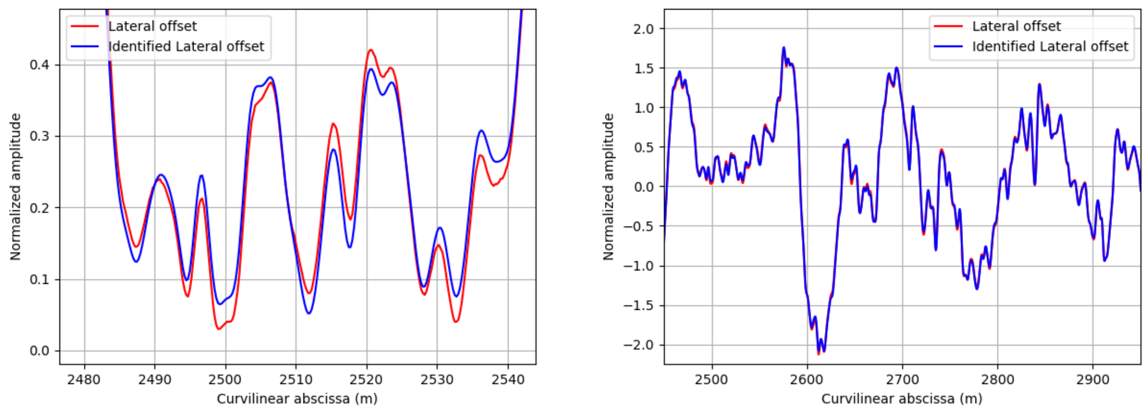

Figure 9: Lateral offset identificatio using the ridge identifie kernel with a half-width of $l = 1000m$

5 CONCLUSIONS

In conclusion, based on the well-known single-axle lateral dynamics model, we have developed a railway dynamics surrogate model that accounts for the presence of a carbody, the track layout, and geometrical irregularities. The resulting system was inverted, and the kinematics of the axle were analyzed, leading to the conclusion that the lateral track irregularity d_3 can be identifie solely using the lateral position of the axle y and its roll θ, both of which can be reconstructed from axle-box accelerations, along with the known curvature of the track γ. Subsequently, the use of these theoretically identifie kernels was compared to kernels derived through linear regression. The next step in this work is to study the stability and sensitivity of the system. Following this, realistic non-linearities will be introduced incrementally, and their impact on the identificatio of the lateral offset irregularity will be analyzed.

REFERENCES

[1] X. Wei, F. Liu, and L. Jia, "Urban rail track condition monitoring based on in-service vehicle acceleration measurements," *Measurement*, vol. 80, pp. 217–228, 2016.

[2] H. Tsunashima, H. Ono, T. Takata, and S. Ogata, "Development and operation of track condition monitoring system using in-service train," *Applied Sciences*, vol. 13, no. 6, 2023.

[3] H. Tsunashima, Y. Naganuma, and T. Kobayashi, "Track geometry estimation from car-body vibration," *Vehicle System Dynamics*, vol. 52, pp. 207–219, 05 2014.

[4] J. S. Lee, S. Choi, S.-S. Kim, C. Park, and Y. G. Kim, "A mixed filterin approach for track condition monitoring using accelerometers on the axle box and bogie," *IEEE Transactions on Instrumentation and Measurement*, vol. 61, no. 3, pp. 749–758, 2012.

[5] E. Bongini and C. Funfschilling, "Procédé et installation d'analyse automatique de l' évolution de la géométrie de voies de circulation," July 2017.

[6] S. Iwnicki, *Handbook of Railway Vehicle Dynamics*. CRC Press, 2006.

[7] V. K. Garg and R. V. Dukkipati, *Dynamics of Railway Vehicle Systems*. Academic Press, 1984.

[8] K. Knothe and S. Stichel, *Rail Vehicle Dynamics*. 01 2017.

[9] A. H. Wickens, "The dynamics of railway vehicles—from stephenson to carter," *Proceedings of the Institution of Mechanical Engineers, Part F: Journal of Rail and Rapid Transit*, vol. 212, no. 3, pp. 209–217, 1998.